# Modelling of ejector chillers with steam and other working fluids

**Modelling of ejector chillers with steam and other working fluids**

Adriano Milazzo*, Andrea Rocchetti

Department of Industrial Engineering, University of Florence, Italy

*Corresponding author. Tel. +39 055 2758738, fax +39 055 2758755, email address:

adriano.milazzo@unifi.it

**Abstract**

The Constant Rate of Momentum Change (CRMC) criterion attempts to improve the design of supersonic ejectors, that can be used in heat-powered chillers for industrial or air-conditioning use. Moving from its original formulation, the CRMC design method can be advanced accounting for friction irreversibilities and real gas behavior, as done in a previous work by our research group. Here we present an upgraded version of this analysis, supported by experimental data from a prototype chiller using R245fa as working fluid. The analysis is extended to other fluids (water, isobutane, 6 HFCs and 3 HFOs) whose performance is calculated on a wide range of heat source/sink temperatures. The existing literature, based generally on ideal gas simulations, suggests that water yields poor results in terms of COP. This paper shows that this result may be argued. Low GWP fluid HFO1233zd also gives good results.

**Keywords**

Ejector chiller; Jet pump; Thermodynamic simulation; Refrigerants; GWP

## Nomenclature

| | | | |
|---|---|---|---|
| $A$ | Area, $m^2$ | Subscripts | |
| $c$ | Velocity, m $s^{-1}$ | $A$ | Condenser exit |
| $D$ | Diameter, mm | $C$ | Condenser |
| $f$ | Friction factor | $CC$ | Cooling cycle |
| $h$ | Specific enthalpy, kJ $kg^{-1}$ | $crit$ | Critical |
| $L$ | Length, m | $E$ | Evaporator |
| $l$ | Work per unit mass, kJ $kg^{-1}$ | $G$ | Generator |
| $M$ | Mass, kg | $irr$ | due to irreversibilities |
| $\dot{m}$ | Flow rate, kg $s^{-1}$ | $mix$ | Mixing section |
| $P$ | Pressure, Pa | $mol$ | Molar |
| $Q$ | Heat power, kW | $p$ | Primary flow |
| $q$ | Heat per unit mass, kJ $kg^{-1}$ | $pump$ | Generator feed pump |
| $s$ | Specific entropy, kJ $kg^{-1}$ $K^{-1}$ | $S$ | Heat source |
| $T$ | Temperature, K | $s$ | Secondary flow |
| $W$ | Power, kW | $sh$ | Superheating |
| $w$ | Velocity, m $s^{-1}$ | $sub$ | Subcooling |
| $x$ | Abscissa, m | $TE$ | Thermal engine |
| $y$ | vapour quality | Abbreviations | |
| Greek symbols | | $CRMC$ | Constant Rate of Momentum Change |
| $\alpha$ | Maximum diffuser angle | $ER$ | Entrainment ratio |
| $\Delta$ | Difference | $GWP$ | Global Warming Potential |
| $\eta$ | Efficiency | $HFO$ | Hydro-Fluoro-Olefines |
| $\xi$ | wall absolute roughness, µm | $NBP$ | Normal Boiling Point |
| $\rho$ | density, kg $m^{-3}$ | $ODP$ | Ozone Depletion Potential |
| $\omega$ | Entrainment ratio | $TEWI$ | Total Equivalent Warming Impact |

## 1. Introduction

Among various available technical options for heat powered cooling systems (absorption, adsorption, etc.), ejector chillers are likely to play a significant role, thanks to their simple, robust and environmentally safe operation (Chen et al. 2013).

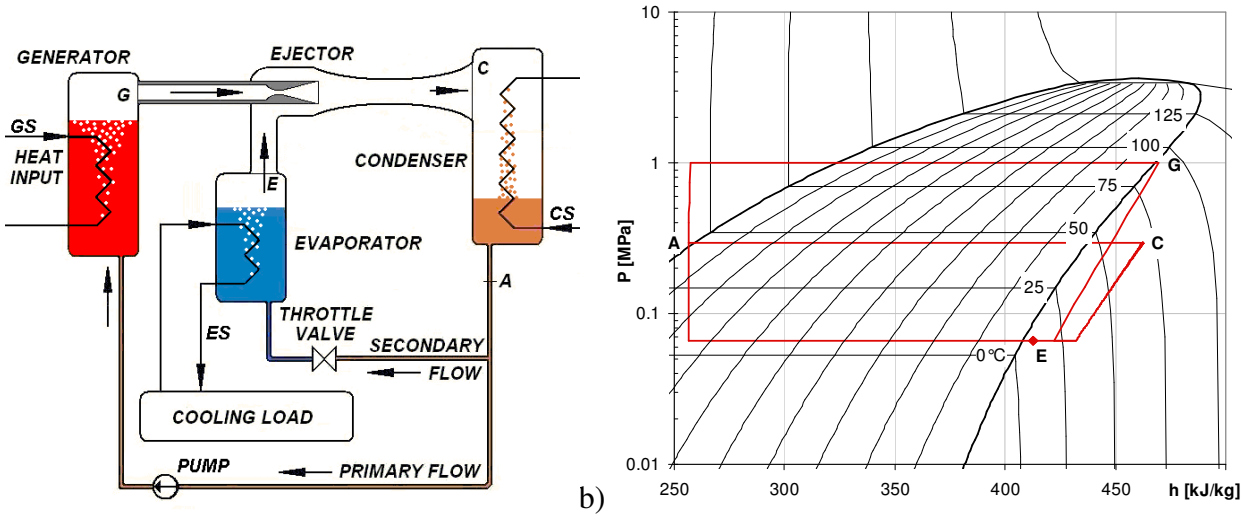


Fig. 1 – Ejector chiller: a) Basic scheme and b) thermodynamic cycle (fluid = R245fa)

In its basic configuration (Fig. 1a), an ejector chiller comprises 3 heat exchangers, an ejector, a pump and an expansion valve. The primary flow runs through a thermal engine cycle AGC to convert the heat input received at the generator into kinetic energy at the primary nozzle exit, whilst the secondary flow (of the same fluid) uses this kinetic energy in the ejector, replacing the compressor in the refrigeration cycle AEC. The two cycles share the condenser, that must therefore discharge the sum of their waste thermal powers. System performance is measured by the ratio between cooling and motive power, i.e. :

$$COP = \frac{Q_f}{Q_{in} + W_{pump}} = \omega \frac{h_E - h_A}{h_G - h_A} \qquad (1)$$

$\omega = \dot{m}_s / \dot{m}_p$ being the "entrainment ratio" between secondary and primary flow rates. The enthalpy differences are visualized for R245fa, as an example, in Fig. 1b.

The enthalpy difference ($h_G - h_A$) in Eq. 1 simply adds the pump work and the heat exchanged at the generator, notwithstanding their different thermodynamic and economic values. For given operating temperatures, the system COP is proportional to $\omega$, which depends on the ejector geometry, operating conditions and working fluid, and to a ratio of enthalpy differences which depends only on the fluid.

Fluid selection is an important and non trivial task. The working fluid in an ejector cycle withstands a wide range of temperatures. Fluid charge is higher in comparison with vapour compression refrigerators, which makes problematic the use of costly or dangerous fluids. Besides, liquid fluid must be pumped from the condenser exit to feed the vapour generator. The feed pump is prone to cavitation and, for certain working fluids, must be able to deliver fluid at high pressure. Pumping power can be quite high if pump efficiency is low.

Starting from the fundamental paper (Dorantes, Lallemand 1995) which used ten chloro and hydro-fluoro-carbons, many authors have considered pure fluids as well as azeotropic or non-azeotropic mixtures as candidate fluids for ejector refrigerators. Sun (1999) compared eleven refrigerants including water, halocarbon compounds, a cyclic organic compound and an azeotrope. Optimum ejector area ratios and COPs were computed for each fluid, concluding that ejectors using R134a and R152a perform well, regardless of operating conditions.

Cizungu et al. (2001) simulated a refrigeration system using a one-dimensional ideal gas model. Theoretical model validation was carried out on R11 and COPs were obtained for four fluids (R123, R134a, R152a, and R717) with different operating conditions and area ratios. For low grade heat source, R134a and R152a achieved higher COP.

Five refrigerants (R134a, R152a, R290, R600a, and R717) were considered by Selvaraju and Mani (2004) within a one-dimensional computer simulation, thermodynamic fluid properties being obtained through REFPROP library. The best performance was found for R134a.

Using empirical correlation from the literature, comparison of COPs for a solar powered ejector refrigeration system operating with eight different working fluids was made by Nehdi et al. (2008), mainly focusing on overall system efficiency and obtaining the best performance for R717.

Petrenko (2009) asserted that R245fa, R245ca, R600 and R600a offer low environmental impact, good performance and moderate generator pressure. This last feature makes feed pump selection easier. Kasperski and Gil (2014) concentrated on hydrocarbons, showing that R600a yields good performance. Varga et al. (2013) confirmed the validity of this fluid.

Wang et al (2014) introduced in the simulations the real properties of refrigerants calculated via REFPROP thermodynamic libraries. They compared R141b, R123, R600a, R142b, R134a, R152a, R290 and R717, concluding that the latter yields the highest COP.

Chen et al. (2014) compared R134a, R152a, R245fa, R290, R600, R600a, R1234ze, R430A and R436B, accounting for the effect of superheating of the primary flow. According to their simulation, R245fa and R600 have the highest COP.

Our research group, in a previously published paper (Grazzini et al. 2012), presented a comprehensive thermodynamic model of an ejector refrigerator. The model structure and its

peculiarities were extensively described therein. Among the various features, the ability to model different working fluids accounting for their real-gas behaviour was claimed. Meanwhile, experimental activity is ongoing and its results, published in (Mazzelli and Milazzo 2015), allow model validation on a specific fluid (R245fa). The model is hence extended to other fluids and the results are discussed herein.

## 2. Selection of the working fluids

Favourable features of a working fluid for an ejector refrigerator are:

- Zero ODP and low GWP;
- Low flammability and toxicity;
- High latent heat and high density at generator, condenser and evaporator temperatures, in order to reduce system size and cost.

From an environmental point of view, it could be noted that ejector chillers may be perfectly sealed (the only moving part, the feed pump, may have a magnetic coupling between rotor and electric motor). Therefore, fluid leakage can be moderate or zero. On the other hand, the fluid charge per unit cooling power is large, yielding potentially high damage in case of accidental release. In Europe, F-gas regulations will ban the use of refrigerants with GWP > 2500 (as R227ea and R236fa) by 2017. This value may hence be set as a threshold.

A set of candidate fluids is listed in table 1. Once ammonia is excluded owing to its toxicity and $CO_2$ for its very low critical point, the first and rather obvious choice is water. Costless and absolutely safe, it has a very high latent heat throughout the typical range of temperatures encountered in ejector cycles. Major drawbacks are the very low pressure and density of steam at cold temperatures and the rather high triple point that impedes low temperature applications.

A second possibility is given by hydrocarbons, that play a central role in the domestic refrigeration market. Iso-butane (R600a) is taken here as an example of this class of fluids, that share low GWP and rather high COP in vapour compression cycles. Isobutane has a “dry expansion” i.e. its entropy decreases along the upper limit curve, which is useful to avoid condensation within the ejector. The obvious burden of hydrocarbons is flammability, which may represent a serious problem as the fluid charge increases.

A third group includes the fluorocarbons. These fluids have zero or low flammability and favourable thermodynamic properties, but generally high GWP. Some of them have dry expansion. Among fluorocarbons, R134a, has a reasonable cost and is well known in the refrigeration industry, but has a high saturation pressure at generator temperature and a relatively high GWP.

Table 1 – Relevant data for a set of zero-ODP fluids

| Fluid | $M_{mol}$ [kg/kmol] | $T_{crit}$ [K] | $P_{crit}$ [MPa] | N.B.P.* [K] | Expansion | GWP | Safety |
|---|---|---|---|---|---|---|---|
| **water** | 18.015 | 647.1 | 22.064 | 373.12 | W | 0 | A1 |
| **R600a** | 58.122 | 407.81 | 3.629 | 261.4 | D | 20 | **A3** |
| **R134a** | 102.03 | 374.21 | 4.059 | 247.08 | W | 1300 | A1 |
| R143a | 84.041 | **345.86** | 3.761 | 225.91 | W | **4300** | A2L |
| **R152a** | 66.051 | 386.41 | 4.517 | 249.13 | W | 120 | **A2** |
| R218 | 188.02 | **345.02** | 2.64 | 236.36 | D | **8600** | A1 |
| R227ea | 170.03 | 374.9 | 2.925 | 256.81 | D | **3500** | A1 |
| **R236ea** | 152.04 | 412.44 | 3.502 | 279.34 | D | 1200 | A1 |
| R236fa | 152.04 | 398.07 | 3.2 | 271.71 | D | **9400** | A1 |
| **R245fa** | 134.05 | 427.16 | 3.651 | 288.29 | D | 950 | B1 |
| R32 | 52.024 | **351.26** | 5.782 | 221.5 | W | 550 | A2L |
| **R365mfc** | 148.07 | 460.0 | 3.266 | 313.3 | D | 890 | - |
| R41 | 34.033 | **317.28** | 5.897 | 194.84 | W | 97 | - |
| RC318 | 200.03 | 388.38 | 2.778 | 267.18 | D | **10000** | A1 |
| **R1234yf** | 114.04 | 367.85 | 3.382 | 243.66 | D | 4 | A2L |
| **R1234ze** | 114.04 | 382.52 | 3.636 | 254.19 | D | 6 | A2L |
| **R1233zd** | 130.5 | 438.75 | 3.772 | 195.15 | D | <5 | A2L |

W=Wet, D=Dry expansion  * Normal Boling Point (P = 101.3 kPa)

$M_{mol}$, $T_{crit}$, $P_{crit}$ and N.B.P. from NIST Refprop; GWP from Calm, Hourahan (2001); Safety from ASHRAE (2008)

R143a, R218, R227ea, R236fa and RC318, are discarded due to their GWP > 2500. R152a has low GWP, but is flammable. R236ea and R245fa have GWP < 2500 and dry expansion. R32 and R41 have moderate GWP, but very low critical temperature. R365mfc has the highest critical temperature, acceptable GWP and dry expansion.

The 3 fluids at the bottom are fluoro-olefins, promising alternatives to fluorocarbons with low GWP and generally low flammability, though likely to have a high cost in the near future.

Everything considered, the 10 fluids in bold characters in Table 1 are retained for further analysis.

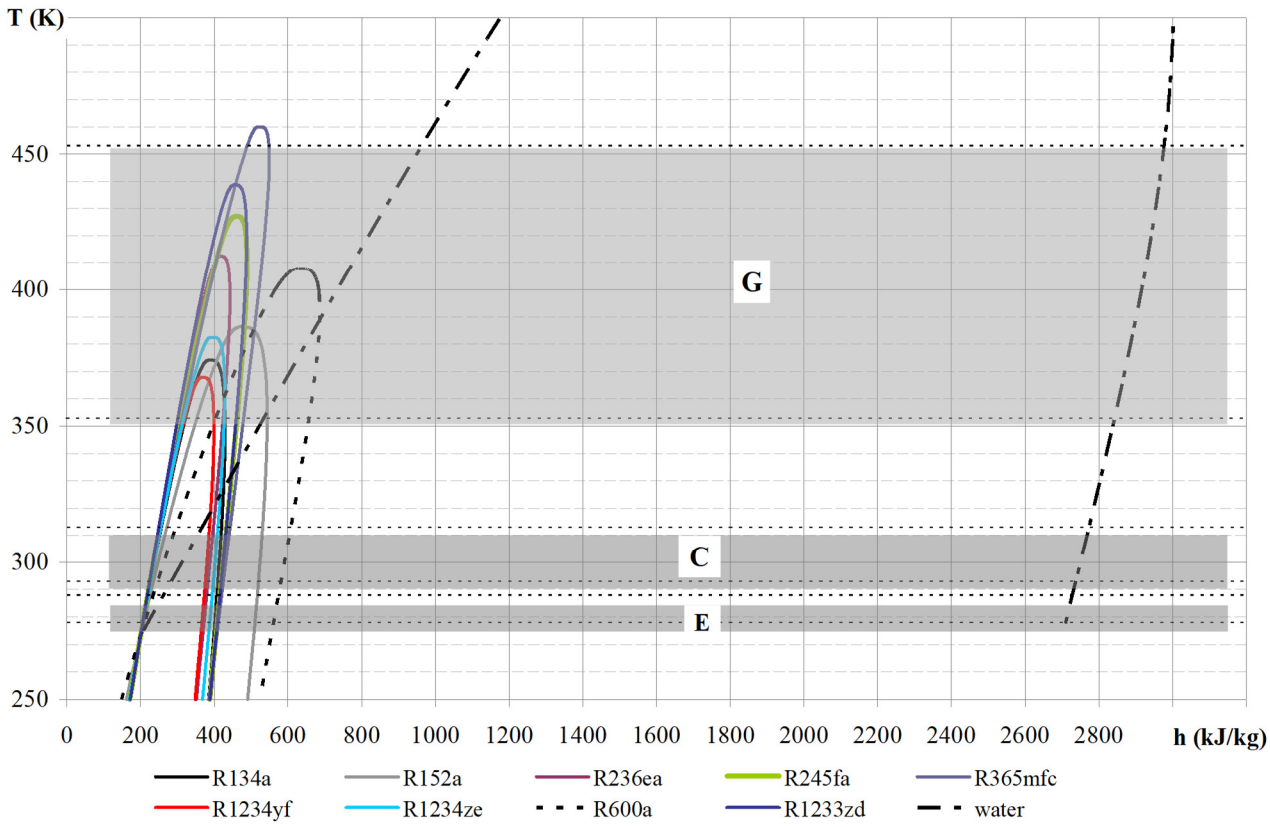


Fig. 2 – Th diagrams for the selected fluids

Fig. 2 shows a *Th* diagram for all fluids, highlighting the temperature ranges of the heat sources that will be discussed later on. Enthalpy is set to 200 kJ $kg^{-1}$ for all fluids at 0°C (IIR reference state), which is unusual for water, but useful here for comparison purposes. Saturation curves are calculated through NIST Refprop subroutines (NIST 2013). The same subroutines, which are provided with a front-end Visual Basic module and can be incorporated in Excel worksheets, were used throughout the thermodynamic simulation. The *Th* diagram is useful to show the energy exchange capability of the various fluids across the temperature range of interest. Water has a 4 to 6 times wider range of latent heat values, leaving the isobutane far on the left. Fluorocarbons and fluoro-olefins form a bundle of hardly distinguishable curves that cover a very short interval on the *h*-axis (200 - 300 kJ $kg^{-1}$). Some of them also show very low critical temperatures.

## 3. Thermodynamic model

The ejector is simulated accounting for real gas behaviour. Therefore, the well-known relations normally used for nozzle design are unusable. Hence the throat section is found from the calculation of the maximum product (density × velocity) along the non-isentropic expansion. Experimental data

(Mazzelli, Milazzo 2015) have been used to evaluate an efficiency of 0.95 for the expansion in the primary nozzle, and this value is used for all fluids.

The whole mixing zone is assumed to be at the same pressure as the evaporator. This assumption differs from the approach adopted in (Grazzini et al. 2012) and in other relevant literature (e.g. Huang et al. 1999), that postulates an adiabatic expansion of the secondary fluid from the evaporator state down to a significantly lower mixing pressure. However, the CFD analysis and experimental results from our R245fa prototype (Mazzelli, Milazzo 2015) show that the mixing pressure is actually close to the evaporator pressure. The secondary flow does accelerate before mixing, but this is not at the expense of its pressure, as would happen in a solid duct. Rather, the secondary flow moves in a "virtual duct" between the outer ejector wall and the expansion cone of the primary jet, where mass and momentum transfer takes place. The mixing process could be examined by a two-dimensional analysis, as attempted e.g. in (Zhu et al., 2007), but for now the aforementioned approach seems adequate and well supported by CFD and experimental evidence.

The mixing loss is simulated through a mixing efficiency defined, as customary in the ejector modelling literature (see e.g. Huang 1999), as the ratio between momentum values behind and before mixing. A value of 0.912 for this efficiency was inferred for R245fa from the aforesaid experimental results and was applied to all fluids, though obviously the fluid features influence the mixing process.

The shape of the mixer/diffuser duct is dictated by the CRMC criterion (Eames, 2002), i.e. the mixed stream momentum is reduced by a constant rate per unit length of the duct. This produces a continuous shape that should eliminate or at least reduce the shock within the cylindrical mixing chambers featured by most ejectors. The First Law of Thermodynamics applied to a small control volume along a straight horizontal duct yields:

$$wdw + dh = \delta q - \delta l \tag{2}$$

The heat exchanged may be found through the Second Law:

$$\delta q = T\left(ds - ds_{irr}\right) \tag{3}$$

while the enthalpy difference may be evaluated along any reversible transformation as $dh = Tds + dP/\rho$. When $dh$ and $\delta q$ are substituted in Eq. 2, the two $Tds$ terms cancel out. The entropy increase due to irreversibility, $ds_{irr}$, is caused by the fluid viscosity and for a length $dx$ of control volume having an approximately constant diameter $D$ may be expressed as:

$$Tds_{irr} = f\frac{dx}{D}\frac{w^2}{2} \tag{4}$$

where $f$ is a friction factor that may be evaluated by the Churchill (1977) formula as a function of Reynolds number and wall roughness. Substitution in equation (2) yields:

$$w dw + \frac{dP}{\rho} + f \frac{dx}{D} \frac{w^2}{2} = 0 \tag{5}$$

A further relation is provided by mass flow conservation:

$$\frac{d\rho}{\rho} + \frac{dw}{w} + \frac{dA}{A} = 0 \tag{6}$$

Combination of equations 5 and 6, after some rearrangement, gives:

$$\frac{dA}{dx} = \frac{A}{w}\left(\frac{d\rho}{dP} w^2 - 1\right)\frac{dw}{dx} + f \frac{A}{D} \frac{d\rho}{dP} \frac{w^2}{2} \tag{7}$$

This formula is slightly different from that used in (Grazzini et al. 2012) because it does not rely on the Mach number. This is useful when the fluid enters the two-phase zone, where definition of the sound speed is not straightforward. Eq. 7 is valid as far as the integration step *dx* is short enough to give negligible variations of diameter *D* and thermodynamic parameter $d\rho / dP$. The latter is evaluated on a very short isentropic compression (*dP* = 1Pa) near the current thermodynamic state.

Once the velocity reduction rate *dw/dx* is given by the CRMC criterion, Eq. 7 can be used to design the diffuser, either for the supersonic (converging) or subsonic (diverging) part. However, when the flow is subsonic the area increases with a growing rate until, in the diffuser tail, the CRMC gives a local slope very likely to cause recirculation at the wall. Therefore, the procedure was modified imposing that the divergence angle do not exceed 5°. Equation 7 is still valid, but the variation rate is imposed for the diffuser diameter instead of velocity. This produces a straight cone that connects the CRMC profile to the ejector outlet, as shown in Fig. 3.

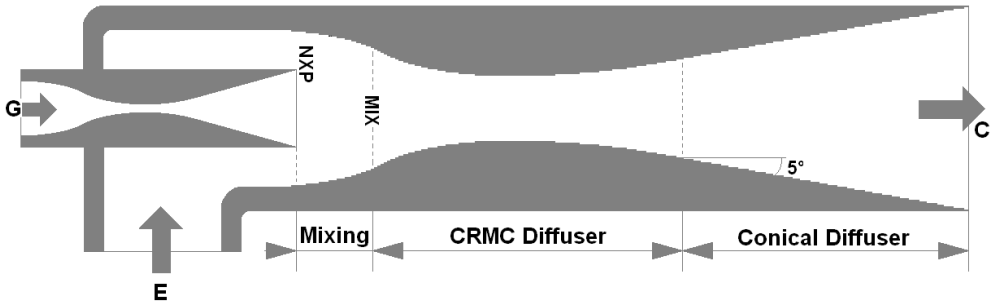


Fig. 3 – Scheme of the ejector

Either imposed or calculated from equation 7, the velocity reduction rate *dw/dx* can be substituted in equation 5 to give the pressure variation:

$$\frac{dP}{dx} = \rho\left(-w\frac{dw}{dx} - \frac{f}{D}\frac{w^2}{2}\right) \tag{8}$$

and in equation 2, simplified for $\delta q = \delta l = 0$, yielding the enthalpy variation:

$$\frac{dh}{dx} = -w\frac{dw}{dx} \tag{9}$$

Once pressure and enthalpy are known on each control volume, NIST routines give all other thermodynamic properties. The procedure ends when the pre-set minimum value of condenser inlet velocity is reached, yielding the diffuser length and exit diameter.

Note that the pressure variation along the duct calculated according to the said procedure is continuous, i.e. without any shock. In practice this is difficult to obtain unless very precise and constant setting of inlet conditions could be obtained. However, the procedure is useful in order to compare the different fluids in the same ideal condition.

The code works iteratively by setting a trial value of entrainment ratio and calculating the diffuser exit pressure. This value is increased/decreased until convergence with the condenser pressure imposed as input data. In this way, the ejector is designed to have the given condenser pressure as the critical value.

## 4. Input data

The simulation code uses the input data listed in Table 2 to calculate the relevant cycle points. The calculation is performed at a steady state corresponding to the maximum condenser pressure allowed by the given working conditions. Pressure loss in the heat exchangers is neglected, in order to separate the effect of fluid selection on the ejector from other effects.

Table 2 - input data

| | | | | | |
|---|---|---|---|---|---|
| $W$ | thermal power at generator [kW] | 90 | $\Delta T_{sh\text{-}E}$ | superheating at evaporator exit [°C] | 5 |
| $T_{GS}$ | hot source at generator inlet [°C] | 80-180 | $\Delta T_{sh\text{-}G}$ | minimum superheating at generator exit [°C] | 5 |
| $T_{CS}$ | ambient source at condenser inlet [°C] | 25-40 | $\Delta T_{sub\text{-}C}$ | subcooling at condenser exit [°C] | 3 |
| $T_{ES}$ | cold source at deliver [°C] | 5-15 | $\eta_p$ | primary expansion efficiency | 0.950 |
| $\Delta T_G$ | ΔT at generator [K] | 3 | $\eta_{mix}$ | mixing efficiency | 0.912 |
| $\Delta T_C$ | ΔT at condenser [K] | 3 | $\eta_{pump}$ | feed pump efficiency | 0.75 |
| $\Delta T_E$ | ΔT at evaporator [K] | 2 | $\alpha$ | maximum diffuser angle [°] | 5 |
| $\xi$ | wall absolute roughness [μm] | 5 | $w_C$ | condenser inlet velocity [m/s] | 10 |

Henceforth reference will be made to the temperature levels of heat sources / sinks introduced in Fig. 1, i.e. hot fluid inlet in the generator ($T_{GS}$), ambient fluid inlet in the condenser ($T_{CS}$) and cold

fluid delivered from the evaporator ($T_{ES}$). The saturation temperature within each heat exchanger is chosen according to the set approach temperature difference (see Table 2 and Fig. 4).

On the cold side, issuing at air conditioning or industrial applications, chilled fluid delivery temperature varies from $T_{ES}$ = 5 to 15°C (range "E" in Fig. 2). Return temperature is 5°C higher.

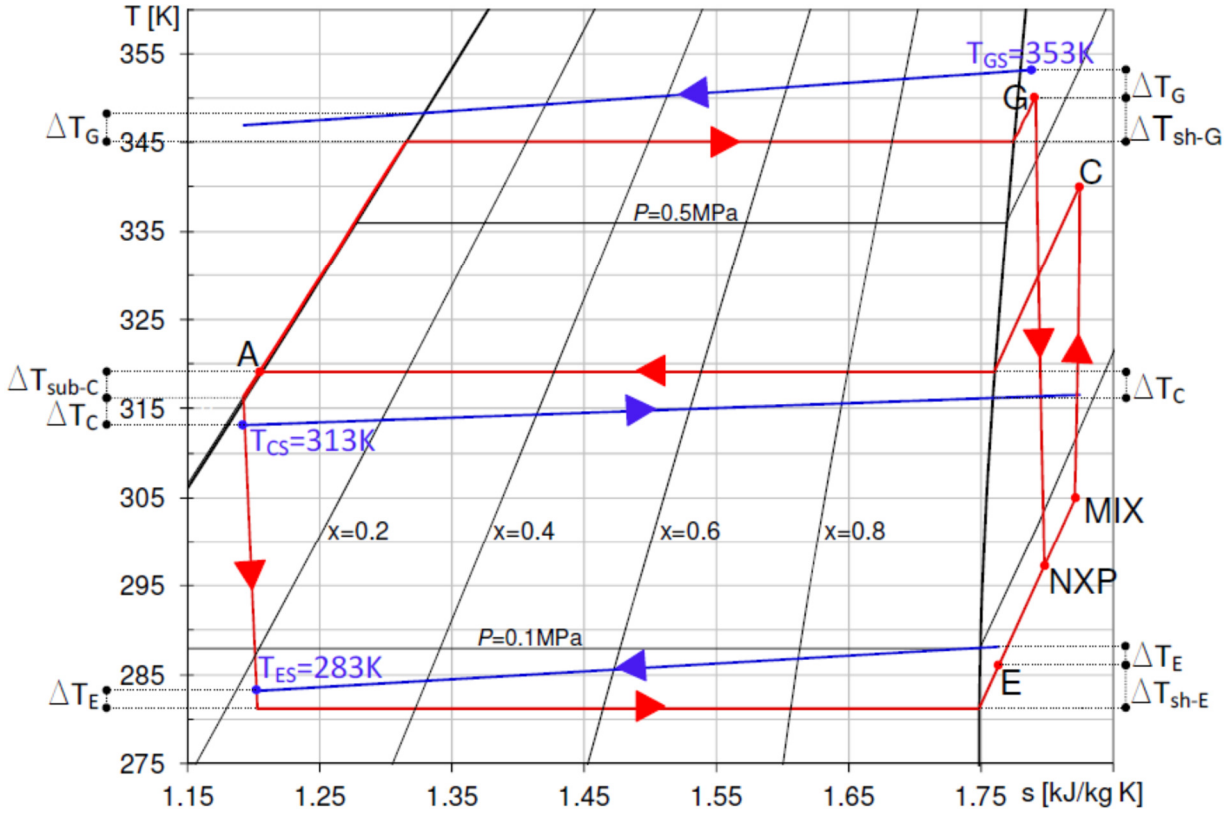


Fig. 4 – Ts diagrams for R245fa at $T_{GS}$=80°, $T_{CS}$=40°C and $T_{ES}$=10°C

The heat source may range from a moderate temperature (e.g. flat solar collectors or district heating/cooling) to rather high temperature (e.g. combined heat, power and cooling fed by engine exhaust). Therefore, the hot fluid temperature at generator inlet is varied from $T_{GS}$ = 80°C to 180°C in the simulations (range "G" in Fig. 2).

The ambient temperature may vary according to the location and time of the year. For stationary applications, likely values range from $T_{CS}$ = 25 to 40°C (range "C" in Fig. 2).

Fixed values are set for approach and pinch point temperature differences within all heat exchangers. Condenser subcooling, evaporator superheating and generator thermal power are also fixed. The saturation temperature and superheating at generator exit are found from a combination of constraints which will be explained in detail later on.

## 5. Results

Before discussing any specific result, it is worth remembering that the simulation program produces a different ejector for each condition, designing its geometry in order to have the maximum entrainment ratio (and hence COP) for given boundary conditions. This means that the operating point stays at the critical condenser pressure for the given generator and evaporator saturation temperatures.

At generator exit, a minimum superheating of 5°C is set for all fluids. Furthermore, a minimum distance is prescribed between the saturation temperature and the critical point, in order to avoid a trans-critical cycle. Looking as an example at R134a in Fig. 5, as $T_{GS}$ increases the generator pressure increases as well, until for $T_{GS}$ > 100°C it remains constant. Superheating must hence be increased, e.g. for R1234yf up to 90°C at $T_{GS}$=180°C. The same applies also to all other fluids except R365mfc, that has higher critical temperatures and remains at 5°C of superheating. As a side effect of the minimum distance imposed between saturation and critical temperature, the generator pressure is kept below 4 MPa for all fluids.

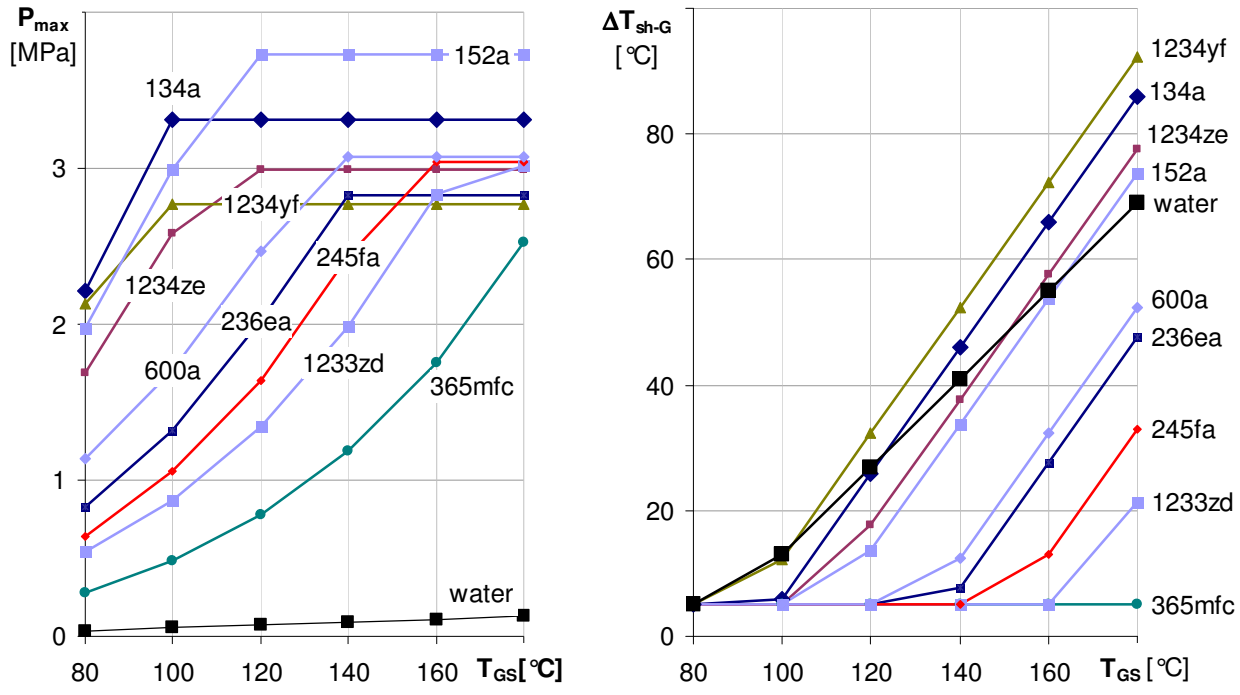


Fig 5 – Saturation pressure and superheating at generator v/s hot source temperature

Another minimum level of superheating is due to the need to maintain a minimum quality (here set to ***y* = 0.85)** at primary nozzle exit. This is necessary for wet fluids, especially for water that would otherwise produce large amounts of liquid within the nozzle. In order to obey this constraint, as shown in Fig. 5, steam has a superheating at generator exit that reaches 70°C at $T_{GS}$=180°C. Also R134a and

R152a at low $T_{GS}$ have wet steam at the primary nozzle exit, but the minimum quality encountered are 0.98 and 0.93 respectively.

Fig. 5 also highlights the remarkably low generator pressure featured by water.

Fig. 6 shows the cycle COP v/s generator temperature, for fixed evaporator and condenser temperatures. Note that these results account for pump work, assuming a constant efficiency $\eta_{pump} = 0.75$ for all fluids and all working conditions. The lowest COP values pertain to R134a and its low-GWP substitutes R1234ze and R1234yf. These fluids show peak COPs ranging between 0.21 and 0.27 in the 100–120°C generator temperature range. A second group of fluids collects R152a, R600a and R236ea, showing peaks between 120 and 140°C with maximum COP values from 0.3 to 0.35. R245fa and R1233zd have peaks at $T_{GS}$ =160°C, the latter fluid reaching the highest value in the graph (COP = 0.42). For all these fluids, the COP starts declining as the constraint on saturation temperature at generator becomes effective. The two fluids with higher critical temperature (water and R365mfc) have increasing COPs through the whole graph.

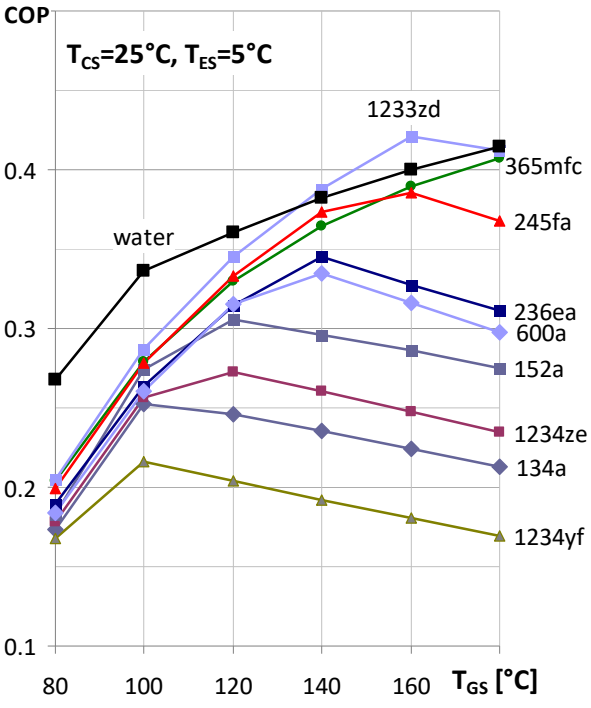


Fig. 6 – COP v/s hot source temperature for $T_{CS}$ = 25°C and $T_{ES}$ = 5°C

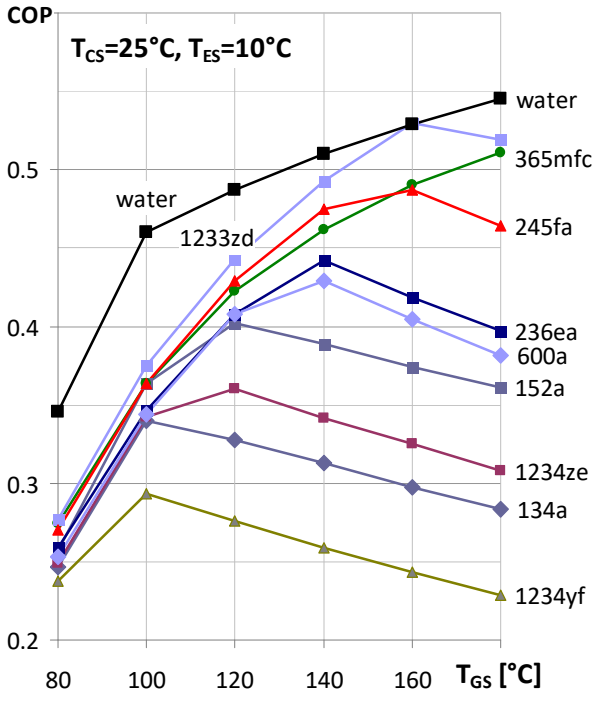


Fig. 7 – COP v/s hot source temperature for $T_{CS}$ = 25°C and $T_{ES}$ = 10°C

The curve pertaining to water has a markedly different shape, with a moderate but stable increase above $T_{GS}$ = 100°C, where the limit on nozzle-end quality comes into effect. Its COP values are higher at low or very high generator temperature, although water is overcome by the peak featured by R1233zd in the 140–180°C range.

As expected, if the evaporator temperature is raised to 10°C, all COP values increase as well. The basic shape of the diagram (Fig. 7) is unchanged, but now water has constantly a higher COP than any other fluid, apart from the single point at $T_{GS}$=160°C where R1233zd has its peak COP and touches the water curve.

If, on the other hand, the condenser temperature is raised, the results worsen. The calculation was made by increasing $T_{CS}$ by 5°C steps and the curve shapes are basically similar. Fig. 8 shows only the highest value used for simulation, $T_{CS}$ = 40°C. Note the interrupted curves featured by some fluids on the lower part of the graph: at such a high condenser temperature, these fluid require a minimum generator temperature of 100°C. Above $T_{GS}$ = 110°C the curve for water is now below those of R1233zd, R365mfc and R245fa, but again is still rising at $T_{GS}$ = 180°C, showing that water would probably overcome any other fluid at very high generator temperatures, given its outstandingly high critical temperature.

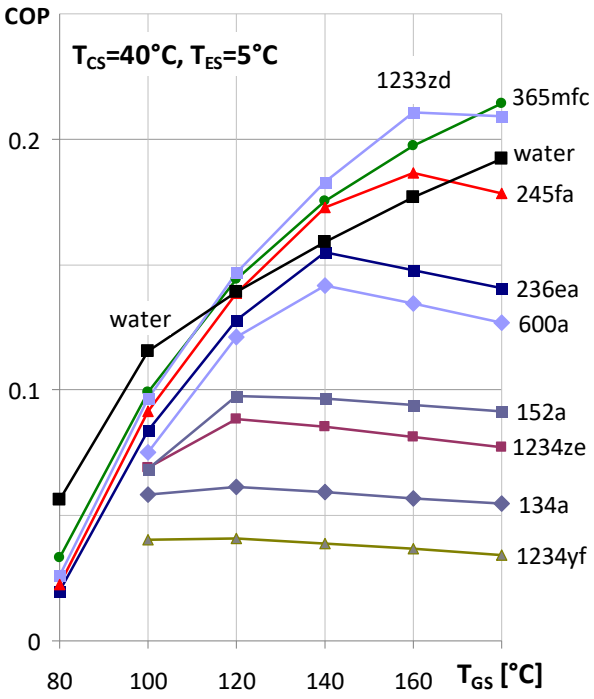


Fig. 8 – COP v/s hot source temperature for $T_{CS}$ = 40°C and $T_{ES}$ = 5°C

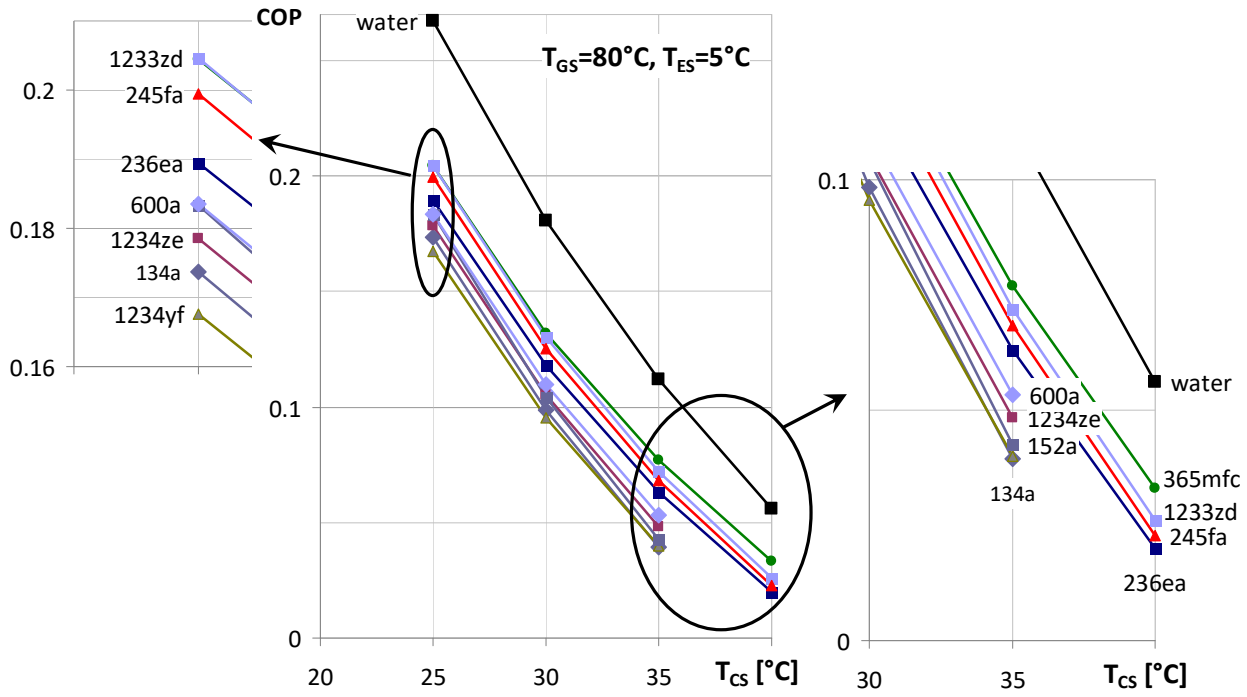


Fig. 9 – COP v/s intermediate source temperature for $T_{GS}$ = 80°C and $T_{ES}$ = 5°C

The same results can be presented as a function of $T_{CS}$ as shown in Fig. 9. At low generator temperature, 5 fluids (R600a, R1234ze, R152a, R134a and 1234yf) have a maximum condenser temperature of 35°C. The other 4 synthetic fluids arrive at $T_{CS}$ = 40°C and show quite similar COP values, R1233zd and R365mfc staying on top at low and high condenser temperatures respectively. Water, at such a low generator temperature, has by far the highest COP at any $T_{CS}$.

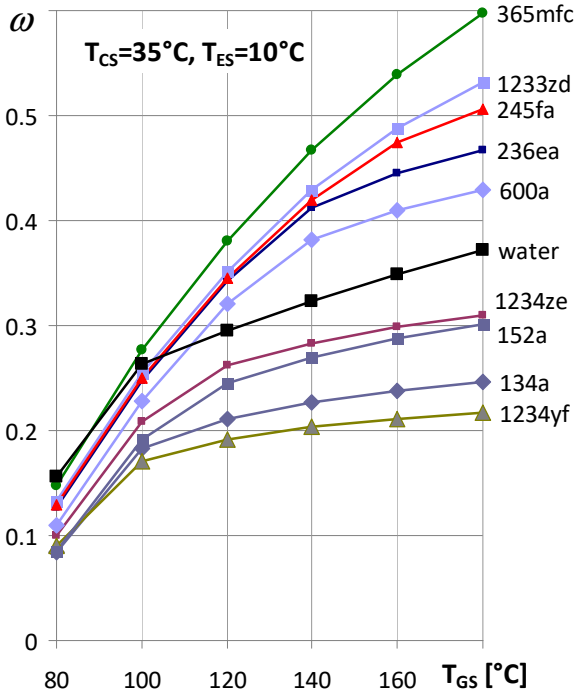


Fig. 10 – Entrainment ratio v/s hot source temperature for $T_{CS}$ = 35°C and $T_{ES}$ = 10°C

In order to understand the above results, a fundamental parameter is the entrainment ratio $\omega$. A single case is shown in Fig. 10, all others being similar. Two circumstances are evident: all curves are monotone and water, for $T_{GS}$>120°C, has moved to the lower part of the diagram. This shows that the enthalpy difference ratio appearing on the right of Eq. 1 should not be neglected. Water may give a lower entrainment ratio, but the favourable shape of the enthalpy diagram overcomes the effect of this parameter and, in many situations, gives a higher performance.

A further insight may be gained by scrutiny of Eq. 1. From a global energy balance of the ejector (assuming negligible variations of kinetic and potential energy at the inlets and outlet, and an adiabatic wall)

$$\omega = \frac{h_G - h_C}{h_C - h_E} \tag{8}$$

Therefore:

$$COP = \frac{h_G - h_C}{h_C - h_E}\frac{h_A - h_E}{h_G - h_A} = \frac{h_G - h_C}{h_G - h_A}\frac{h_A - h_E}{h_C - h_E} = K_1 K_2 \tag{9}$$

Subscripts A, C, E and G refer to the working fluid states as defined in Fig. 1.

In the last member of Eq. 9, the system COP is written as the product between two factors $K_1$ and $K_2$. In this way the different fluid features may be isolated, highlighting how each fluid behaves respectively in the upper and lower portion of the cycle.

For example, Fig. 11 shows the factor $K_1$ in the same working conditions as Fig. 10. All curves increase. The poor performance of water is evident. The high latent heat, in this case, increases the heat input between points A and G, while the enthalpy difference between points G and C is comparable to that of the other fluids. The best performance is registered by R365mfc.

An opposite situation is highlighted for factor $K_2$ in Fig. 12. All curves now decrease, but the outstanding performance of steam makes the others hardly distinguishable. In this case the high latent heat is very advantageous, as it increases the cooling capacity $h_A$ - $h_E$, while the enthalpy input $h_C$ - $h_E$ is comparable with the other fluids.

In the end, the product of the two factors may vary in a difficultly predictable way, as shown in Figs. 6-10.

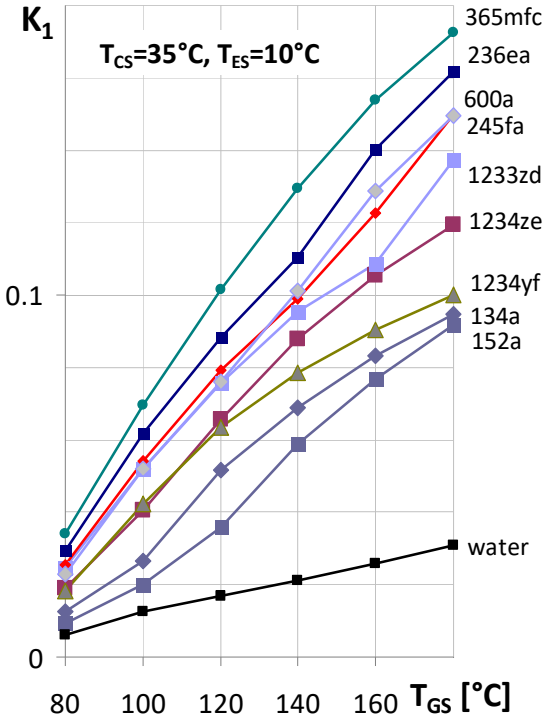


Fig. 11 – Factor $K_1$ ($T_{CS}$ = 35°C, $T_{ES}$ = 10°C)

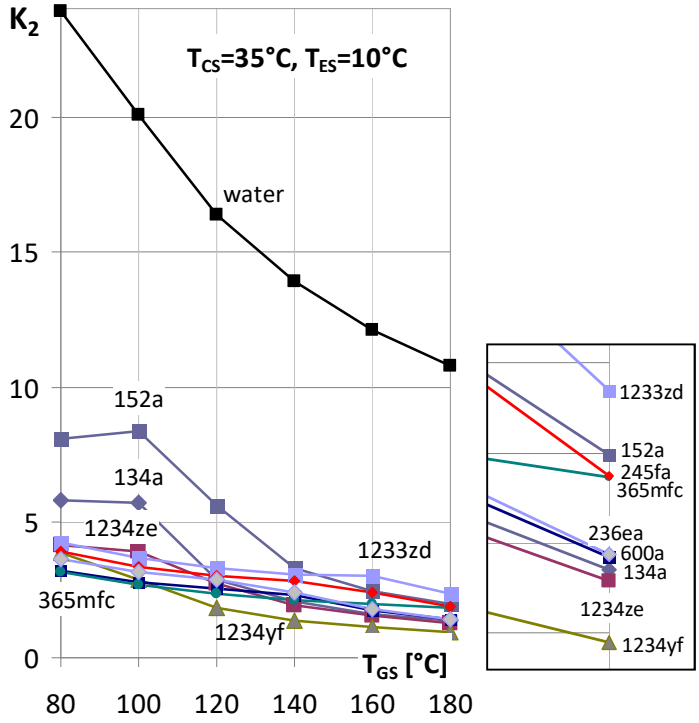


Fig. 12 – Factor $K_2$ ($T_C$ = 35°C, $T_E$ = 10°C)

## 5. Discussion

The results shown in Fig. 4-8 are quite different from others reported in the relevant literature. For example Varga et al. (2013) place water invariably at the bottom in all COP diagrams. A possible reason for this evident discrepancy may be in their model, which recalls the classic one-dimensional, ideal gas scheme presented by Huang et al. (1999). In the case of steam, given the very high latent heat of condensation, even small amounts of condensed water may heavily affect the state of the expanding fluid. In a previous paper (Grazzini et al. 2011) it was shown that an ideal gas expansion between typical generator and evaporator pressure levels would reach temperature values near 100 K and nucleation theory does foresee the presence of droplets within the nozzle. Similar remarks are found in (Ariafar et al. 2014), where nucleation is introduced in a CFD simulation and the difference from a ideal gas simulation are highlighted.

The results shown in the present paper, postulate an equilibrium state. This may be a significant departure from reality, but the results may be regarded as an opposite boundary delimiting real fluid behaviour: the ideal gas, on the one hand, postulates the fluid properties to be frozen throughout the expansion, while the equilibrium two-phase fluid is supposed to follow the expansion with no delay. The real fluid will stay somewhere in between and other tools (e.g. Wilson curves) may be used to describe its metastable behaviour. Here, however, the analysis focuses on fluid comparison and more refined simulations are postponed.

The occurrence of condensation within the ejector requires a more complex model, accounting for two-phase flow. However, homogeneous nucleation during a fast expansion produces very small droplets that should closely follow the streamlines of the gaseous phase. The minimum quality limit ($y = 0.85$) assumed herein is taken from the established practice of steam turbines, i.e. is commonly accepted in presence of moving blades, so it should not pose unbearable troubles in an ejector.

Given the low generator pressure and the high density, water may even be fed by gravity, eliminating the pump (Nguyen et al. 2001).

High specific volume at evaporator and condenser may well increase the size of these heat exchangers, but this can be a minor problem for fixed installations. The high triple point of water can cause icing problems, but may even turn out to be an opportunity, as shown by Eames et al. (2013) who integrated an ice storage system within an ejector chiller.

By the way, the review of experimental results presented by Chen et al. (2013) shows that water has the highest COP together with R134a. The cited value (0.48) was measured by Chunnanond and Aphornratana (2004) at $T_E = 10°C$ and $T_G = 120°C$.

## 5. Conclusions

The thermodynamic simulation code for ejector chillers presented in this paper has some original features, i.e. it eliminates the ideal gas assumption and calculates the diffuser as a continuous profile, accounting for distributed loss through a friction factor. Empirical efficiencies are used only for the primary nozzle and the mixing process, their value being validated by experiments on a R245fa ejector.

In the paper, 10 fluids are compared on a wide range of working conditions (80-180°C for the higher heat source, 20-40°C for the intermediate and 5-10°C for the lower). Water shows a good performance, especially at generator temperatures below 120°C. For example, an ejector chiller working on a hot source at 100°C, a cold source at 5°C and an ambient source at 25°C would give COP=0.34 with water and COP=0.28 with R245fa. This result disagrees with others published in the recent literature. The discrepancy can be justified by the inclusion of condensation within our model, as opposite to other papers that rely on ideal gas simulations and hence reach thermodynamic states that, in the case of water, are rather unrealistic.

Water also features a saturation pressure at generator which is at least one order of magnitude lower in comparison to any other fluid, allowing a lighter and cheaper construction.

High COP is also obtained by the low-GWP fluid R1233zd, that could be an interesting alternative, though obviously the fluid cost is much higher in comparison with steam.

**Aknowledgements**

The present research is part of a joint research project involving Frigel Firenze S.p.A.

**References**

Ariafar, K., Buttsworth, D., Sharifi, N., Malpress, R., 2014, Ejector primary nozzle steam condensation: Area ratio effects and mixing layer development, Appl. Therm. Eng. 71, 519–527

ASHRAE, 2008. Addenda to Designation and safety classification of refrigerants, ANSI/ASHRAE Standard 34-2007.

Calm, J.M., Hourahan, G.C., 2001. Refrigerant data summary. Eng. Syst.18(11), 4–88.

Chen, X., Omer, S., Worall, M., Riffat, S., 2013. Recent developments in ejector refrigeration technologies. Renew. Sust. Energy Rev.19, 629–651.

Chen, J., Havtun, H., Palm, B., 2014. Screening of working fluids for the ejector refrigeration system. Int. J. Refrig. 47, 1–14.

Chunnanond, K., Aphornratana, S., 2004. An experimental investigation of a steam ejector refrigerator: the analysis of the pressure profile along the ejector. Appl. Therm. Eng. 24, 311–322.

Churchill, S.W., 1977. Friction-factor equation spans all fluid-flow regimes. Chem Eng. 7, 91–92.

Cizungu, K., Mani, A., Groll, M., 2001. Performance comparison of vapour jet refrigeration system with environment friendly working fluids. Appl. Therm. Eng. 21, 585–598.

Dorantes, R., Lallemand, A.. 1995. Prediction of performance of a jet cooling system operating with pure refrigerants or non-azeotropic mixtures. Int. J. Refrig. 18, 21–30.

Eames, I.W., 2002. A new prescription for the design of supersonic jet-pumps: the constant rate of momentum change method. Appl. Therm. Eng. 22, 121–31.

Eames, I.W., Worall, M., Wu, S., 2013. An experimental investigation into the integration of a jet-pump refrigeration cycle and a novel jet-spay thermal ice storage system. Appl. Therm. Eng. 53, 285–290.

Eames, I.W., Milazzo, A., Paganini, D., Livi, M., 2013b. The design, manufacture and testing of a jet-pump chiller for air conditioning and industrial application. Appl. Therm. Eng. 58, 234–240

Grazzini, G., Milazzo A., Piazzini, S., 2011. Prediction of condensation in steam ejector for a refrigeration system. Int. J. Refrig. 34, 164-648.

Grazzini, G., Milazzo A., Paganini D., 2012. Design of an ejector cycle refrigeration system. Energy Convers. Manag. 54, 38–46.

Huang, B.J., Chang, J.M., Wang, C.P., Petrenko, V.A., 1999. A 1-D analysis of ejector performance. Int. J. Refrig. 22, 354–364.

Kasperski, J., Gil, B., 2014. Performance estimation of ejector cycles using heavier hydrocarbon refrigerants. Appl. Therm. Eng. 71, 197–203

Mazzelli, F., Milazzo, A., 2015. Performance analysis of a supersonic ejector cycle working with R245fa. Int. J. Refrig., 49., 79 – 92.

Milazzo, A., Rocchetti, A., Eames, I.W., 2014. Theoretical and experimental activity on Ejector Refrigeration. Energy Procedia 45, 1245 – 1254.

Nehdi, E., Kairouani, L., Elakhdar, M., 2008. A solar ejector air-conditioning system using environment-friendly working fluids. Int. J. Energy Research 32, 1194–1201.

Nguyen, V.M., Riffat, S.B., Doherty, P.S., 2001. Development of a solar-powered passive ejector cooling system. Appl. Therm. Eng. 21, 157–168.

NIST Standard Reference Database. <http://www.nist.gov/srd/nist23.cfm> (accessed 03.11.2014).

Petrenko, V.O., 2009. Application of innovative ejector chillers and air conditioners operating with low boiling refrigerants in trigeneration systems. In: International Seminar on ejector/jet-pump technology and application, Louvain-la-Neuve, Belgium.

Selvaraju, A., Mani, A., 2004. Analysis of an ejector with environment friendly refrigerants. Appl. Therm. Eng. 24, 827–838.

Sun, D-W., 1999. Comparative study of the performance of an ejector refrigeration cycle operating with various refrigerants. Energy Convers. Manag. 40, 873–884.

Varga, S., Lebre, P.S., Oliveira, A.C., 2013. Readdressing working fluid selection with a view to designing a variable geometry ejector. Int. J. Low-Carbon Techn. 0, 1–11.

Wang, F., Shen, S.Q., Li, D.Y., 2014. Evaluation on environment friendly refrigerants with similar normal boiling points in ejector refrigeration system. Heat Mass Transfer, Springer.

Zhu, Y., Cai, W., Wen, C., Li, Y., 2007. Shock circle model for ejector performance evaluation. Energy Convers. Manag. 48, 2533–2541.